

ExpRDiff: Short-exposure Guided Diffusion Model for Realistic Local Motion Deblurring

Zhongbao Yang Jiangxin Dong Jinhui Tang Jinshan Pan
School of Computer Science and Engineering, Nanjing University of Science and Technology
<https://github.com/yzb1997/ExpRDiff>



Figure 1. Deblurring images with real-world local motion blur. The left side shows examples of a long-exposure photo (top) and a short-exposure photo (bottom) of the same scene captured by smart phones with vivo X100 pro. Both existing local blur removal methods, e.g., LBAG [10], and state-of-the-art image deblurring methods, e.g., NAFNet [3], do remove local blur well as shown in (a) and (c). In addition, simply using the short exposure image as reference does not solve this problem well, as shown in (b). In contrast to existing methods, we develop an effective ExpRDiff to explore the sharp information from the shortexposure images and blur information from the blurred images for blur removal and use them to guide the diffusion models for better realistic image restoration.

Abstract

Removing blur caused by moving objects is challenging, as the moving objects are usually significantly blurry while the static background remains clear. Existing methods that rely on local blur detection often suffer from inaccuracies and cannot generate satisfactory results when focusing solely on blurred regions. To overcome these problems, we first design a context-based local blur detection module that incorporates additional contextual information to improve the identification of blurry regions. Considering that modern smartphones are equipped with cameras capable of providing short-exposure images, we develop a blur-aware guided image restoration method that utilizes sharp structural details from short-exposure images, facilitating accurate reconstruction of heavily blurred regions. Furthermore, to restore images realistically and visually-pleasant, we develop a short-exposure guided diffusion model that explores useful

features from short-exposure images and blurred regions to better constrain the diffusion process. Finally, we formulate the above components into a simple yet effective network, named ExpRDiff. Experimental results show that ExpRDiff performs favorably against state-of-the-art methods.

1. Introduction

Existing smart phones equipped with anti-shake functions significantly improve the quality of captured images. However, capturing clear moving objects in a dynamic low-light environment is still a difficult problem as a longer exposure time is often required and the speed of the moving objects is fast. The long-exposure photo with significant local blur effects; e.g., the objects are blurry while the static background is usually clear. Thus, how to deblur images with the local blur effect receives significant attention from both academic and industry communities.

Most existing methods are designed mainly for images with a uniform or non-uniform global blur effect [3, 4, 7, 14, 19, 21, 25, 26]. When applying these methods to images with local blur, the clear background will be over smoothed, while moving objects are not restored well. Thus, it is of great need to develop an effective method to handle the clear background and blurry objects simultaneously for better image restoration. To this end, several approaches [10, 11] adopt object segmentation or blur detection approaches to differentiate between blurry and clear regions, subsequently handling blur regions and clear regions simultaneously. However, local blurs resulting from object motion often present significant challenges (e.g., the tire in the blue boxes of the 2st patch in Figure 1), and adverse imaging conditions, such as low-light environments, further increase the difficulty of object segmentation or blur detection. As a result, reliance solely on object segmentation or blur detection does not effectively improve deblurring performance. We note that existing handheld devices can capture multiple photos of a moving object simultaneously through burst mode or multi-camera systems. Photos captured using these settings typically contain sharp details due to the short-exposure times (e.g., the tire in the yellow boxes of the 2st patch in Figure 1). Thus, it is of great interest to explore the information of these images to facilitate local blur removal.

To solve the problems mentioned above, we develop an ExpRDiff to explore information from localized blur regions and short-exposure images as guidance to facilitate local blur removal. First, given that not all the regions of captured images are blurry, we develop a context-based local blur detection module to explore contextual information for better identification of the blurry regions. Then, we develop a simple yet effective blurry-aware guided image restoration that explores the useful information of short-exposure images and the detected blurry regions as guidance to discriminately handle the blurry regions and clear regions simultaneously for better image restoration.

However, as the moving speeds of the objects are usually fast, which leads to significant blur effects, restoring realistic clear images with rich details from heavily blurred images is not a trivial task. Motivated by the success of diffusion-based methods [22, 23] in high-quality image generation, we take advantage of diffusion priors to help with realistic clear image restoration.

To ensure that the diffusion model pays more attention to restoring reliable structural details, we develop a simple yet effective feature fusion module, named ExpBFusion, to adaptively extract useful features from the short-exposure images and the detected blurry regions. These features obtained through ExpBFusion can then guide the diffusion model for better image restoration. By formulating the aforementioned modules into a unified frame-

work, the proposed ExpRDiff achieves favorable performance against state-of-the-art methods on publicly available local blur datasets as well as real-world scenarios.

The main contributions are summarized as follows:

- We develop a context-based local blur detection module to explore additional contextual information to improve the identification of blurry regions.
- We develop a blurry-aware guided image restoration to remove local blur by handling the blurry regions and clear regions discriminately in the restoration process.
- We develop a short-exposure guided diffusion model to explore useful features from the short-exposure images and the detected blurry regions as guidance for realistic image restoration.

2. Related Work

Hand-crafted prior-based methods. Since image deblurring is ill-posed, conventional methods usually use reference images with clearer structural information as effective priors to jointly solve image deblurring. In [2], Chen et al. propose joint image deblurring with two images with different levels of blurring. Zhuo et al. [29] and Yuan et al. [24] to perform image deblurring with the help of flash images and noisy images as reference images, in which the structure is clearer, respectively. Although traditional joint image deblurring methods can achieve better results than traditional single image deblurring methods, traditional joint image deblurring methods assume that the blurring are global of these images can be well described by a single blur kernel result from camera shake and the scene is static. These methods provide poor performance of deblurring in images with non-uniform blurring and blurred images caused by object motion.

Deep learning-based methods. To solve more complex image deblurring situations avoiding the limitations assumed in manually designing image priors, Deep learning-based image deblurring methods are explored to solve image deblurring. Lost of single image deblurring methods [4, 8, 9, 14, 17–19, 21, 27] achieve favorable performance. Zamir et al. [25] propose a multi-stage progressive image deblurring method for the restoration image. The non-parameter sharing network is utilized in different stages to learn the deblurring function of the corresponding scales. While this design achieves competitive performance, the complexity of the model thus becomes larger. To reduce the parameters of the model, Chen et al. [3] propose a computationally efficient simple baseline, which considers the nonlinear activation functions to be non-essential and replaces them. But the amount of convolutional operations makes those CNNs-based methods only have the ability to capture localized information.

With the development of transformer [20] in high-level

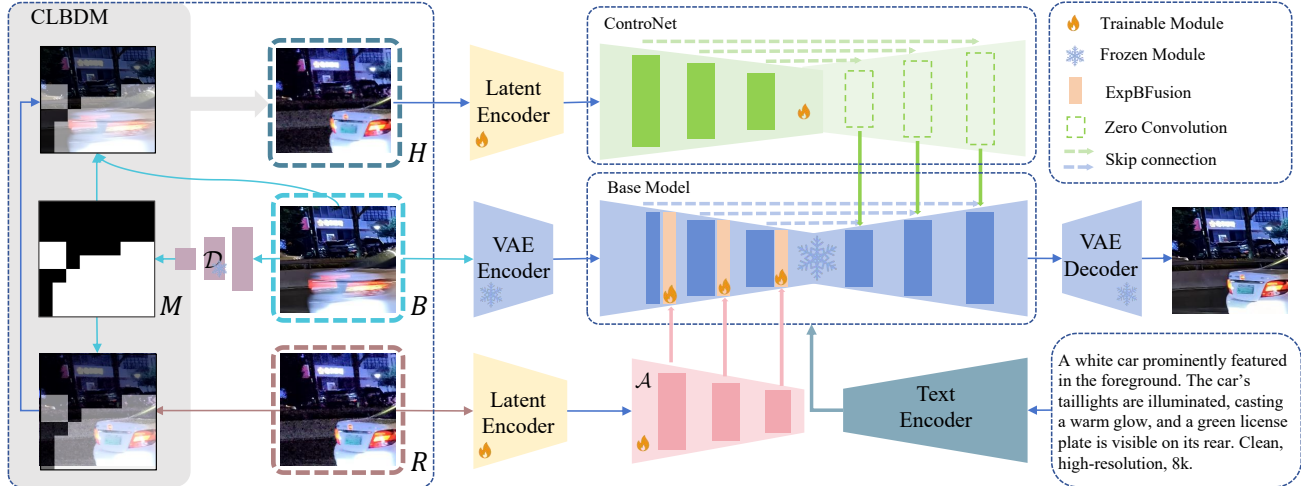


Figure 2. An overview of the proposed method ExprDiff. \mathcal{A} is the network to extract features for R . \mathcal{D} denotes Blurry-aware guided image restoration, which aims to extract short-exposure image features, CLBDM denotes the context-based local blur detection module. B , R , M , and H are blurry images, short-exposure images, confidence maps, and the result of CLBDM respectively.

vision tasks, whose ability to capture global contexts caught the attention to researchers. [26] calculates channel attention and [7] computes the dot-product attention on the spatial frequency domain separately, which reduces the complexity of computing the attention weights in the transformer. [11] propose a window-based local motion deblurring vision transformer network, which employs the confidence predictor that constrains the output at the pixel level using the mask of gt to predict blur areas. The confidence predictor network is trained in such kind of strategy that it leads to mask generation inaccurately.

Diffusion-based image restoration. With the surprising performance of StableDiffusion-XL (SDXL) [16] in image image-generating field, it has been developed for image restoration. To solve the problem of uncontrollable generation of images in the image generation task, [15, 28] employ another branch to extract the features of the condition to control the final generated output. Inspired by that, [12, 22, 23] utilize the degradation network to generate clear images or clear latent from the input degraded images, which is used to put into the denoising model and the ControlNet [28] to control the diffusion process and generate high-quality images.

Although the images recovered by those methods achieve pleasant visualization results, the training of these methods is based on a large collection of high-quality images and utilizes synthetic degraded images, which do not allow for the restoration of local blur caused by object motion. In order to better utilize the prior provided by SDXL to recover local blur in the presence of a reference image, we propose the diffusion-based low-light local motion deblurring network.

3. Proposed Method

The proposed ExprDiff aims to explore useful features from short-exposure images and blurry regions as guidance for local blur removal and realistic image restoration. It contains a context-based local blur detection module that is used to identify blurry regions by exploring contextual information, a blurry-aware guided image restoration that uses the short-exposure images and blurry regions to remove local blur, and a short-exposure guided diffusion model that is constrained by the features of short-exposure images and blurry regions for realistic image restoration. Figure 2 shows the overview of the proposed ExprDiff. In the following, we explain each component in detail.

3.1. Context-based local blur detection module

Local blur detection is an essential step for handling images with local blur. Existing methods [10, 11] usually treat this problem as a binary classification and employ a binary network to determine whether each pixel position is blurry or not. However, this approach, which relies solely on individual pixel characteristics, often fails to capture contextual information, leading to inaccurate blur detection and subsequent degradation in overall result quality. To address this problem, we develop a simple yet effective context-based local blur detection method that incorporates additional contextual information to enhance the robustness of local blur detection.

Specifically, we first divide the input blurry images into N non-overlapping patches $\{P_i\}_{i=1}^N$ with the unfolding operation from the input blurry image B , where $P_i \in \mathbb{R}^{C \times 60 \times 60}$. Then, we develop a simple yet effective network $\mathcal{D}(\cdot)$ to estimate a set of confidence values $\{V_i\}_{i=1}^N$,

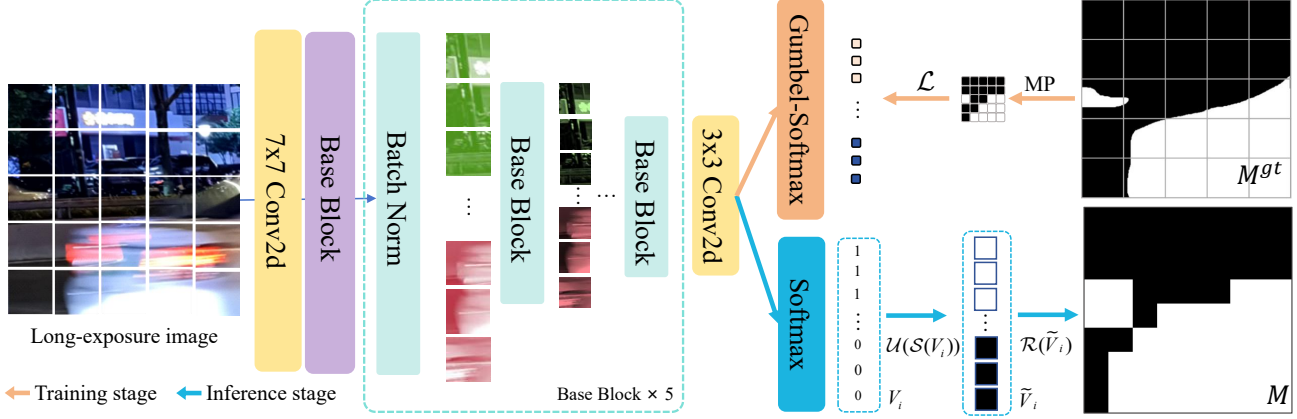


Figure 3. An overview of the proposed context-based local blur detection module to detect the blur regions of the long-exposure blur image. MP denotes the Max-pooling operation.

$V_i \in \mathbb{R}^{C \times 1 \times 1}$, from the input blurry image to discriminate whether the divided patches $\{P_i\}_{i=1}^N$ are blurry or not:

$$V_i = \mathcal{S} \left(\frac{\mathcal{D}(P_i) + G_i}{\tau} \right), \quad (1)$$

where $G_i = -\log(-\log(U_i))$, $U_i \sim \text{Uniform}(0, 1)$, $\mathcal{S}(\cdot)$ denotes the Softmax operation, τ is the temperature parameter that controls the smoothness of the distribution, G_i represents the Gumbel noise added for differentiable sampling [6], and U_i is a random variable sampled from a uniform distribution $\text{Uniform}(0, 1)$. Figure 4 illustrates the detailed architecture of the module.

We train the network \mathcal{D} by minimizing the following Cross-Entropy loss function:

$$\mathcal{L} = -\frac{1}{N} \sum_{i=1}^N [V_i \log(M_i^{gt}) + (1 - V_i) \log(1 - M_i^{gt})], \quad (2)$$

where M_i^{gt} denotes the ground truth confidence map that indicates the blur degree of the patch P_i . It is obtained by cropping the corresponding region from the ground truth blur confidence map M^{gt} based on the spatial position of patch P_i .

As the confidence map is estimated in image patches, we employ the nearest-neighbor interpolation to obtain the pixel-level confidence map M to discriminate the blurry regions and clear regions from input image:

$$\begin{aligned} \tilde{V}_i &= \mathcal{U}(\mathcal{S}(V_i)), \quad V_i \in \mathbb{R}^{C \times 60 \times 60}, \\ M &= \mathcal{R}(\tilde{V}_i), \end{aligned} \quad (3)$$

where $\mathcal{U}(\cdot)$ denotes the nearest-neighbor interpolation operation, $\mathcal{R}(\cdot)$ denotes the folding operation.

In addition to better detection of blurred regions, the confidence map generated by the proposed context-based local

blur detection module further helps short-exposure images guide the recovery of realistic effects in blurred regions. We will show its effectiveness in Section 5.

3.2. Blurry-aware guided image restoration

With the guidance of a short-exposure image, one can use the guided filtering method [5] to help eliminate blur. However, directly using [5] will smooth the clear background as shown in Figure 5. Meanwhile, the short-exposure images in clear regions have poor quality in low-light environments (e.g., the tree in the blue boxes of the 2st patch in Figure 1). A natural solution to this problem is that we do not handle the clear regions of the input images. To this end, we adopt a threshold based on the default value of the Gumbel-Softmax distribution to binarize M . Then, we develop a blurry-aware guided restoration approach that formulates the guided filtering method as:

$$H(x) = M(x)(a_k R(x) + b_k) + (1 - M(x))B(x), \quad x \in w_k, \quad (4)$$

where a_k and b_k are linear coefficients in an image patch w_k ; $B(x)$ and $R(x)$ denote the input blurry image and short-exposure image at pixel x .

The linear coefficients a_k and b_k can be obtained by solving the following optimization problem:

$$\min_{a_k, b_k} \sum_{i \in w_k} (M(x)(a_k R(x) + b_k) + (1 - M(x))B(x) - B(x))^2 + \epsilon a_k^2, \quad (5)$$

where ϵ is a weight parameter. Similar to [5], the solution of a_k and b_k can be obtained:

$$\begin{aligned} a_k &= \frac{\sum_{i \in w_k} M(x_i)^2 R(x_i) B(x_i) - \sum_{i \in w_k} M(x_i)^2 R(x_i) b_k}{\sum_{i \in w_k} M(x_i)^2 R(x_i)^2 + \epsilon}, \\ b_k &= \frac{\sum_{i \in w_k} M(x_i)^2 B(x_i) - \sum_{i \in w_k} M(x_i)^2 a_k R(x_i)}{\sum_{i \in w_k} M(x_i)^2}. \end{aligned} \quad (6)$$

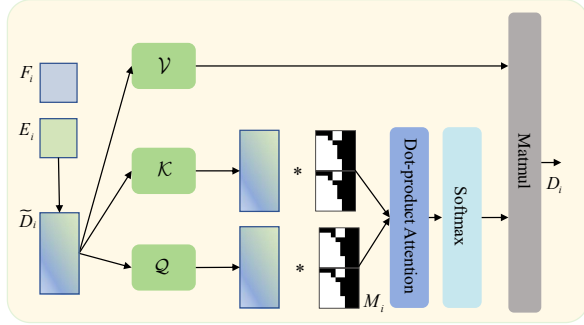


Figure 4. Details of the proposed ExpBFusion module.

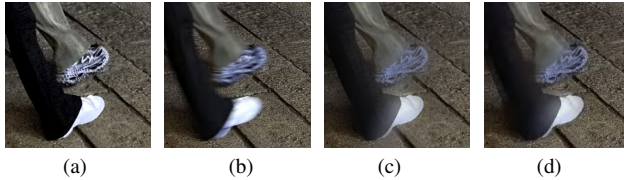


Figure 5. Illustration of guided image filtering [5]. (a) Short-exposure reference; (b) blurred input; (c) result of direct guided filtering, which reduces blur but smooths the static background; (d) result of masked guided filtering, preserving background clarity while achieving the same deblurring effect in blurred regions as (c).

The details about the derivation of Eqs. (6) are included in the supplemental material.

3.3. Short-exposure guided diffusion model

Although the proposed blurry-aware guided image restoration can remove local blur well, it is less effective to restore realistic images with details due to the significant blur caused by moving objects. We note that existing diffusion-based methods with text prompts can recover details from the degraded image. However, text information is a high-level feature and cannot effectively characterize blurry regions and low-level structural features of images. Thus, only using the text prompt does not guide the diffusion models for realistic image restoration when local blur exists. To address this problem, we propose a short-exposure guided diffusion model that explores the features of both short-exposure images and blurry regions for better image restoration.

Specifically, assuming that the multi-scale features $\{E_i\}_{i=1}^s$ are from the encoder module of the U-Net in the diffusion model, where s denotes the number of scales, we first extract the multi-scale features $\{F_i\}_{i=1}^s$ from the short-exposure image by a feature extraction network¹, where the spatial resolution of F_i is the same as E_i .

Then, with the multi-scale features $\{F_i\}_{i=1}^s$ and the esti-

¹The details about the feature extraction network are included in the supplemental material.

mated confidence map M , we develop ExpBFusion, a simple yet effective feature fusion module, to guide $\{E_i\}_{i=1}^s$ in the diffusion process:

$$D_i = \mathcal{S} \left(\frac{\mathcal{Q}(\tilde{D}_i)\mathcal{K}(\tilde{D}_i)^\top}{\gamma} \right) \mathcal{V}(\hat{D}_i), \quad (7)$$

where $\tilde{D}_i = \mathcal{C}(F_i \otimes M_i, E_i \otimes M_i)$ and $\hat{D}_i = \mathcal{C}(F_i, E_i)$; $\mathcal{C}(\cdot)$ denotes a concatenation operation along the spatial dimension; M_i denotes the nearest downsampling result of M , which has the same spatial resolution as F_i ; \otimes denotes the element-wise product operation; $\mathcal{Q}(\cdot)$, $\mathcal{K}(\cdot)$, and $\mathcal{V}(\cdot)$ denote the operations for extracting the query, key, and value matrices, respectively; γ is a learnable weight parameter. Finally, we use the fused feature D_i instead of E_i in the diffusion process. The detailed module is shown in Figure 4 and we employ the base model of StableDiffusion-XL (SDXL) [16] as our diffusion model as it generates high-quality and realistic images. We refer to the module by Eq. (7) as the proposed short-exposure guided diffusion model and show its effectiveness and efficiency in Section 5.

4. Experimental Results

We evaluate the effectiveness of the proposed method against the state-of-the-art ones using public benchmark datasets.

4.1. Experimental settings

Training datasets. We use the ReLoBlur dataset [10] as our training dataset. To generate short-exposure images, we first convert the sharp images into the hue saturation value (HSV) color space to reduce the brightness and add random noise to these images. Then we crop the input images and the corresponding masks with the spatial size of 512×512 pixels to focus on local details. We split the dataset into 19,351 pairs for training and 3,824 for evaluation.

To demonstrate the generalization ability of our proposed method on real-world data, we capture the real local motion blurred dataset (LMBD) that contains 10,380 images for training and 209 images for evaluation. The details are included in the supplemental material.

Parameter settings. We implement our method using the PyTorch framework and train it on a machine with 8 NVIDIA GeForce RTX 4090 GPUs. The AdamW [13] optimizer with default parameters is used. The patch size is set to be 256×256 pixels, and the batch size is 32. We employ the loss function [22] to regularize our network and train the proposed network with 160,000 iterations, The initial learning rate is set to 5×10^{-5} .

Evaluation metrics. How to better evaluate the quality of restored images is important. Note that conventional dis-

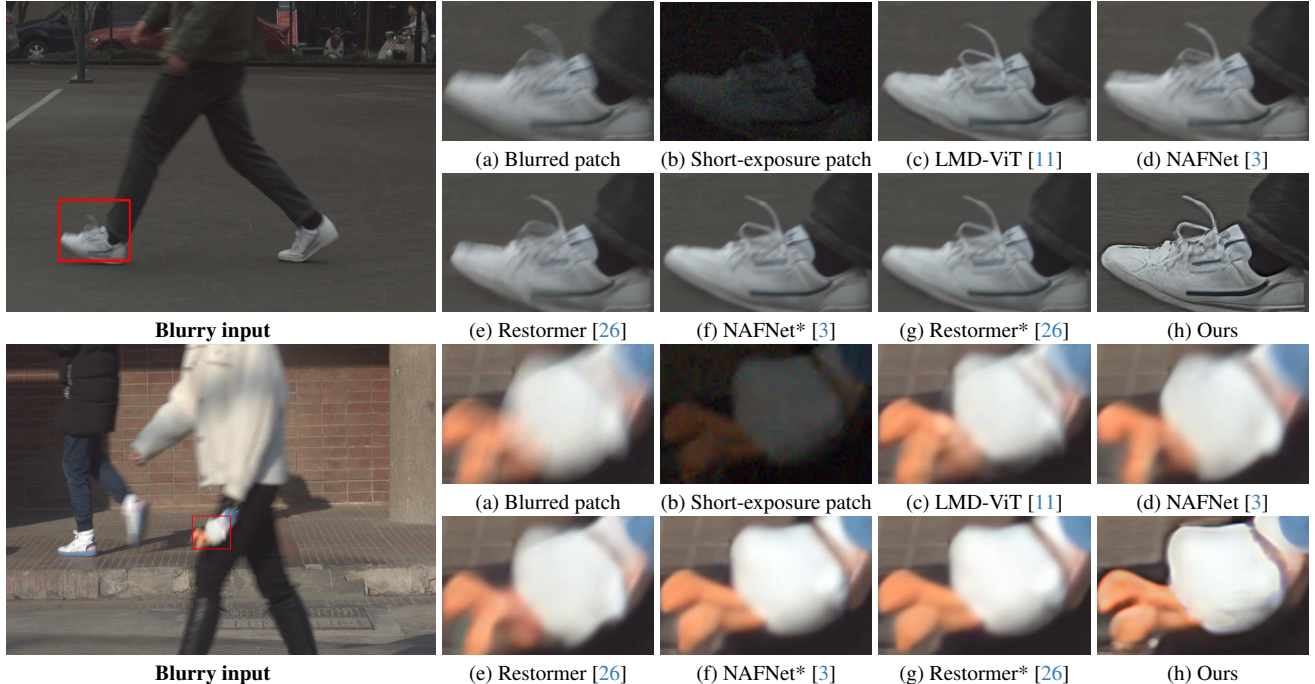


Figure 6. Deblurred results on the ReLoBlur synthetic dataset [10]. The deblurred results in (c)-(g) still contain significant blur effects. The proposed method generates a better deblurred image with clearer structures in (h).

Table 1. Quantitative evaluations of the proposed approach against state-of-the-art methods on the ReLoBlur synthetic dataset [10]. The “*” represents that we concat the R and B as the model input. The \downarrow and \uparrow represent that lower values indicate better results, and higher values indicate better results, respectively.

Methods	NIQE \downarrow	CLIPQA+ \uparrow	MUSIQ-PAQ2PIQ \uparrow
MIMO-UNet [4]	6.1947	0.3525	58.0449
NAFNet [3]	5.9387	0.3631	59.9376
Restormer [26]	6.1146	0.3596	59.2634
MIMO-UNet* [4]	5.9514	0.3607	60.9325
NAFNet* [3]	5.8419	0.3644	61.2459
Restormer* [26]	5.8826	0.3669	61.4244
LBAG [10]	5.9243	0.3644	60.1322
LMD-ViT [11]	5.9341	0.3389	59.8619
Ours	5.2212	0.3709	65.8149

tortion measures, e.g., PSNR and SSIM do not measure the visual quality of images well [1]. We mainly use NIQE, CLIPQA+, and MUSIQ-PAQ2PIQ as the main evaluation metrics as they are able to measure the visual quality of images well.

4.2. Comparisons with the state of the art

To provide a comprehensive evaluation, we also compare it with global deblurring methods such as NAFNet [3], Restormer [26], and MIMO-UNet [4] and local deblurring methods such as LBAG [10] and LMD-ViT [11].

As the proposed method requires a short-exposure image as guidance, one may wonder whether the performance gains are due to the use of additional information. To an-

Table 2. Quantitative evaluations on the LMBD dataset. All the comparison results are generated using the publicly available code and trained on the same training datasets for fair comparisons.

Methods	NIQE \downarrow	CLIPQA+ \uparrow	MUSIQ-PAQ2PIQ \uparrow
MIMO-UNet [4]	9.9320	0.3130	59.8464
NAFNet [3]	9.2736	0.3045	59.7057
Restormer [26]	9.6038	0.3051	60.7811
MIMO-UNet* [4]	8.2208	0.2950	63.6510
NAFNet* [3]	8.2431	0.2977	63.6596
Restormer* [26]	8.5662	0.3127	64.7834
LBAG [10]	10.0196	0.2968	58.5612
Ours	4.3228	0.3531	65.1461

swer this question, we further use the concatenation of the blurry and the short-exposure images as input of the existing methods for comparison.

For fair comparisons, we retrain the evaluated methods on the same training datasets. The values of NIQE, CLIPQA+, and MUSIQ-PAQ2PIQ are tested on images of size 512×512 with locally blurred.

Evaluations on the ReLoBlur synthetic dataset. Table 1 summarizes the quantitative evaluation results, where the proposed method achieves high-quality results with higher NIQE, CLIPQA+, and MUSIQ-PAQ2PIQ values.

Although the global deblurring methods use short-exposure images as reference (e.g., Restormer* [26]), they show improvement in the results compared to when no reference image guidance, the NIQE gain of our method is at least 0.62 better than above methods. In addition, compared

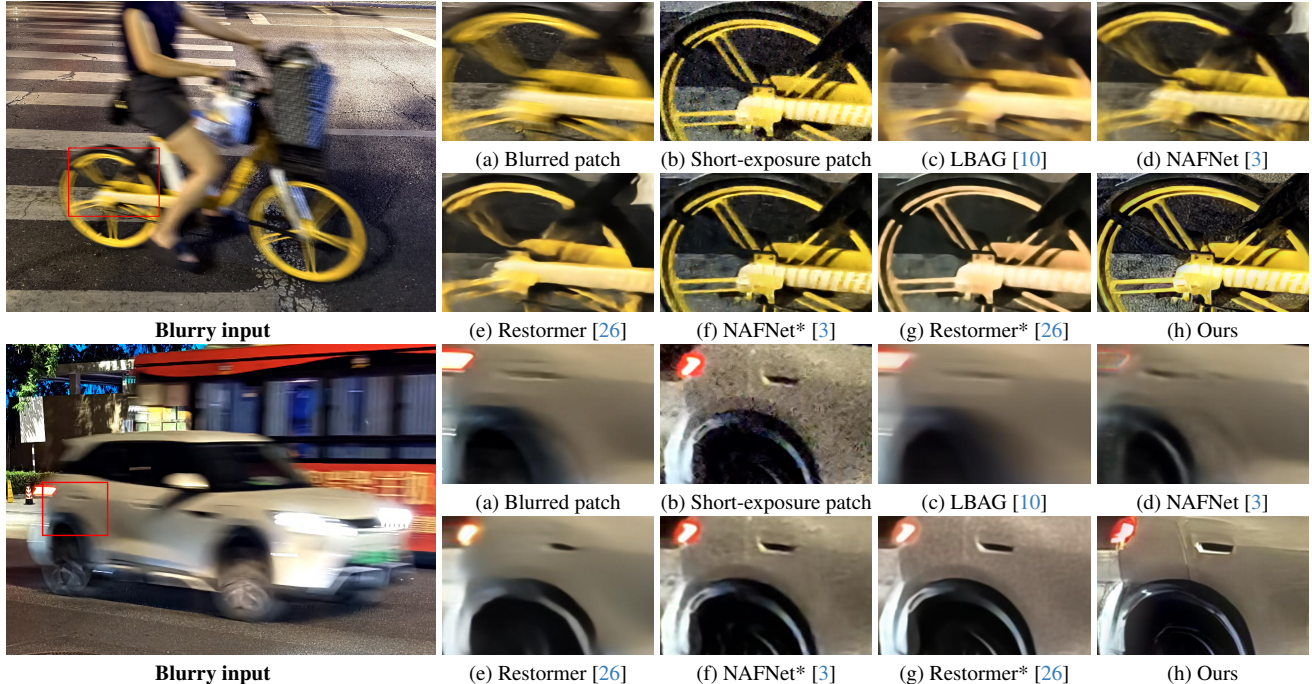


Figure 7. Deblurred results on the LMBD dataset. The deblurred results in (c)-(g) still contain significant blur effects. The proposed method generates a better deblurred image with clearer structures in (h).

Table 3. Effect of the proposed blurry-aware guided image restoration in the proposed method on the LMBD dataset.

Methods	w/o BGF	w/ GF	w/ BGF
CLIPQA+ \uparrow	0.3296	0.2815	0.3395
MUSIQ-PAQ2PIQ \uparrow	62.1051	59.5076	62.4996

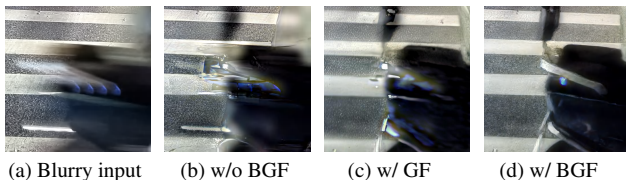


Figure 8. Effectiveness of the proposed blurry-aware guided image restoration on image deblurring.

to the local deblurring methods [10, 11], our method generates better results.

Figure 6 shows that the evaluated methods do not restore the shoes effectively. In contrast, our method generates better results. For example, the shoelaces and boundaries are much clearer.

Evaluations on the LMBD dataset. Table 2 shows the quantitative evaluation results. Our method achieves the highest quantitative results. Compared with global deblurring methods, our method shows a NIQE gain of at least 4.6 better than NAFNet [3]. The above methods use the short-exposure image as the reference, which demonstrate measurable enhancements in their quantitative performance metrics compared to when reference image guidance is not

Table 4. Effect of proposed ExpBFusion in the proposed method on the LMBD dataset.

Methods	w/o F	w/ F & w/o M	w/ F
CLIPQA+ \uparrow	0.3395	0.3368	0.3531
MUSIQ-PAQ2PIQ \uparrow	62.4996	64.7102	65.1461



Figure 9. Effectiveness of the proposed ExpBFusion on image deblurring.

provided.

However, the MUSIQ-PAQ2PIQ gain of our method is at least 0.52 higher than Restormer* [3] and 6.74 higher than local deblurring method LBAG [10]. Figure 7 shows some visual comparisons of the evaluated methods. The global deblurring methods do not remove the blur effects, as shown in Figure 7(c)-(d). Figure 7(f)-(g) are the visual results of the above methods that use the short-exposure image as a reference and are still missing structural information.

In contrast to the above methods, we utilize the priors from diffusion models to assist in the restoration of blurred regions to achieve a refinement effect in the blurred regions. Thus, the deblurred results contain clear structures, and the hub of the tire and the ground appear much clearer as shown in Figure 7(h).

5. Analysis and Discussion

To better understand how our method addresses local motion deblurring with reference images, and demonstrate the effect of its main components, we provide in-depth analysis of the proposed method. For the ablation studies in this section, we train our method and all the baselines on the LMBD dataset using the batch size of 32.

Effect of the blurry-aware guided image restoration.

The proposed blurry-aware guided image restoration is designed to eliminate blur with the guidance of a short-exposure image in blurred regions.

To demonstrate the effectiveness of our proposed blurry-aware guided image restoration, we compare the method utilizing blurry-aware guided image restoration (w/ BGF for short) with the baseline that the method uses long-exposure image (w/o BGF for short) to guide the restoration of the local motion blurred image.

Table 3 shows that the method using the blur-aware guided image restoration generates better deblurring results, where the MUSIQ-PAQ2PIQ value is 0.39 better. Furthermore, we compare the method using the blur-aware guided image restoration with the method using guided filtering method [5] (w/ GF for short). The comparison results table 3 shows that the method using blur-aware guided image restoration generates better results with higher MUSIQ-PAQ2PIQ values. Figure 8 shows that the method using the proposed blur-aware guided image restoration generates better deblurred images, where the motorcycle tail is recovered well shown in Figure 8(d).

Effect of the short-exposure guided diffusion model. The proposed short-exposure guided diffusion model is used to generate realistic results by a fusion module ExpBFusion.

To examine whether ExpBFusion effectively utilizes features from both short-exposure images and blurred regions to guide the diffusion process, we compare our method (w/ F for short) with the baseline that the proposed method without using a short-exposure guided diffusion model (w/o F for short). Table 4 shows that the proposed method using ExpBFusion generates better results, where the MUSIQ-PAQ2PIQ values is 2.80 higher than baseline.

Furthermore, we explore whether utilizing the global sharp information from the short-exposure image to the diffusion process improves the results. To answer this question, we remove the M from the ExpBFusion (w/ F & w/o M for short) as the baseline. Compared with the baseline, our proposed method generates better results, where the MUSIQ-PAQ2PIQ value is 0.44 better.

Figure 9 shows the visualization results. Using the proposed short-exposure guided diffusion model generates better clear images, where the lines of the tires and the ground in the background are clearer.

Table 5. Effect of proposed context-based local blur detection module in the proposed method on the LMBD dataset.

Methods	w/ M^c	w/ M	w/ M^{gt}
CLIPQA+ \uparrow	0.3393	0.3531	0.3571
MUSIQ-PAQ2PIQ \uparrow	64.4785	65.1461	65.3015

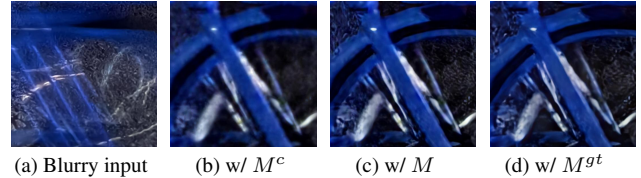


Figure 10. Effectiveness of the proposed blurry-aware guided image restoration on image deblurring. (b) illustrates the restoration results using the method with M^c , which partially enhances image details but still leaves some residual blur.

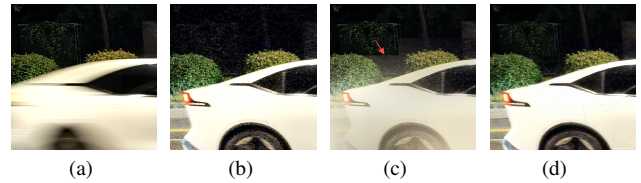


Figure 11. Effectiveness of the proposed short-exposure guided diffusion model on the elimination of boundary artifacts. (a) Blur input; (b) short-exposure reference; (c) result of blurry-aware guided image restoration; (d) result of our method.

We further explore the effectiveness of the proposed short-exposure guided diffusion model in handling the boundary effects caused by the mask. Figure 11(c) shows that after blurry-aware guided image restoration, although the blur has been removed, boundary effects introduced by the mask remain. However, after applying the short-exposure guided diffusion model, the result of our method eliminates the influence of these boundary effects, as shown in Figure 11(d).

Effect of the context-based local blur detection module.

The proposed context-based local blur detection module to improve the identification of blurry regions.

To demonstrate the effectiveness of the proposed context-based blurred regions detection module in our proposed method, we first replace the M with ground truth mask M^{gt} (w/ M^{gt} for short). The result in Table 5 shows that using the mask generated by the context-based blurred regions detection module (w/ M for short) performs Competitive with the ground truth one. Then, we demonstrate the effectiveness of M on ExprDiff. We replace the M with not been binarized confidence map (w/ M^c for short). Table 5 shows that the proposed method achieves better results, where the MUSIQ-PAQ2PIQ value is 0.67 better.

The visual comparisons in Figure 10(c) demonstrate that using the context-based local blur detection module generates results that are competitive compared to the use of ground truth masks.

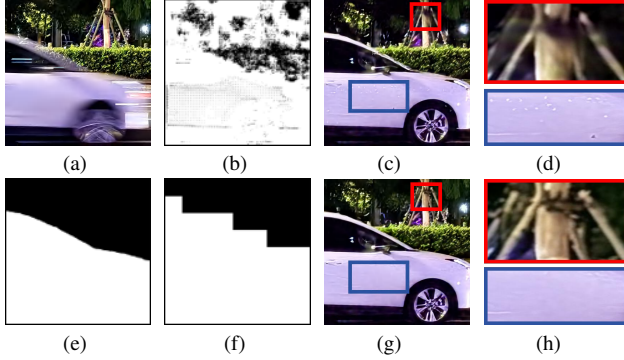


Figure 12. Effectiveness of the context-based local blur detection module in blur region recognition. (a) Blurry input; (b) blurry region identification result of the context-based local blur detection module trained to identify for each pixel blur or not; (c) result of our method generated using the mask in (b); (d) zoomed-in details of the red and blue regions in (c); (e) ground truth mask; (f) blurry region identification result of the pixel-wise based local blur detection module; (g) result of our method generated using the mask in (f); (h) zoomed-in details of the red and blue regions in (g).

We further compare the context-based local blur detection module and the pixel-wise based local blur detection method in terms of their ability to identify blur regions. The method based on pixel information does not identify the blur regions well as shown in Figure 12(b). Figure 12(f) shows that the context-based local blur detection module better identifies blur regions and ultimately helps the model generate better results.

6. Conclusion

We propose ExprDiff to explore features from short-exposure images and blurry regions to guide local blur removal and realistic image restoration. To improve the identification of blurry regions, we design a context-based local blur detection module that incorporates additional contextual information to determine whether the regions are blurry or not. Subsequently, we develop a blur-aware guided image restoration method that utilizes sharp structural details from short-exposure images, facilitating accurate reconstruction of heavily blurred regions. Furthermore, to achieve realistic images with better visually appealing restoration, we present a short-exposure guided diffusion model that utilizes features from both short-exposure images and blurred regions to effectively guide the diffusion process. Experimental results show that ExprDiff performs favorably against the state-of-art methods.

References

[1] Yochai Blau and Tomer Michaeli. The perception-distortion tradeoff. In *CVPR*, 2018. 6
 [2] Jia Chen, Lu Yuan, Chi-Keung Tang, and Long Quan. Robust dual motion deblurring. In *CVPR*, 2008. 2

[3] Liangyu Chen, Xiaojie Chu, Xiangyu Zhang, and Jian Sun. Simple baselines for image restoration. In *ECCV*, 2022. 1, 2, 6, 7
 [4] Sung-Jin Cho, Seo-Won Ji, Jun-Pyo Hong, Seung-Won Jung, and Sung-Jea Ko. Rethinking coarse-to-fine approach in single image deblurring. In *ICCV*, 2021. 2, 6
 [5] Kaiming He, Jian Sun, and Xiaoou Tang. Guided image filtering. In *ECCV*, 2010. 4, 5, 8
 [6] Eric Jang, Shixiang Gu, and Ben Poole. Categorical reparameterization with gumbel-softmax. In *ICLR*, 2017. 4
 [7] Lingshun Kong, Jiangxin Dong, Jianjun Ge, Mingqiang Li, and Jinshan Pan. Efficient frequency domain-based transformers for high-quality image deblurring. In *CVPR*, 2023. 2, 3
 [8] Orest Kupyn, Volodymyr Budzan, Mykola Mykhailych, Dmytro Mishkin, and Jiri Matas. Deblurgan: Blind motion deblurring using conditional adversarial networks. In *CVPR*, 2018. 2
 [9] Orest Kupyn, Tetiana Martyniuk, Junru Wu, and Zhangyang Wang. Deblurgan-v2: Deblurring (orders-of-magnitude) faster and better. In *ICCV*, 2019. 2
 [10] Haoying Li, Ziran Zhang, Tingting Jiang, Peng Luo, Huajun Feng, and Zhihai Xu. Real-world deep local motion deblurring. In *AAAI*, 2023. 1, 2, 3, 5, 6, 7
 [11] Haoying Li, Jixin Zhao, Shangchen Zhou, Huajun Feng, Chongyi Li, and Chen Change Loy. Adaptive window pruning for efficient local motion deblurring. In *ICLR*, 2024. 2, 3, 6, 7
 [12] Xinqi Lin, Jingwen He, Ziyang Chen, Zhaoyang Lyu, Bo Dai, Fanghua Yu, Wanli Ouyang, Yu Qiao, and Chao Dong. Diffbir: Towards blind image restoration with generative diffusion prior. *arXiv preprint arXiv:2308.15070*, 2023. 3
 [13] Ilya Loshchilov and Frank Hutter. Decoupled weight decay regularization. In *ICLR*, 2019. 5
 [14] Xintian Mao, Yiming Liu, Wei Shen, Qingli Li, and Yan Wang. Deep residual fourier transformation for single image deblurring. *CoRR*, abs/2111.11745, 2021. 2
 [15] Chong Mou, Xintao Wang, Liangbin Xie, Yanze Wu, Jian Zhang, Zhongang Qi, and Ying Shan. T2i-adapter: Learning adapters to dig out more controllable ability for text-to-image diffusion models. In *AAAI*, 2024. 3
 [16] Dustin Podell, Zion English, Kyle Lacey, Andreas Blattmann, Tim Dockhorn, Jonas Müller, Joe Penna, and Robin Rombach. SDXL: improving latent diffusion models for high-resolution image synthesis. In *ICLR*, 2024. 3, 5
 [17] Maitreya Suin, Kuldeep Purohit, and A. N. Rajagopalan. Spatially-attentive patch-hierarchical network for adaptive motion deblurring. In *CVPR*, 2020. 2
 [18] Xin Tao, Hongyun Gao, Xiaoyong Shen, Jue Wang, and Jiayia Jia. Scale-recurrent network for deep image deblurring. In *CVPR*, 2018.
 [19] Fu-Jen Tsai, Yan-Tsung Peng, Yen-Yu Lin, Chung-Chi Tsai, and Chia-Wen Lin. Stripformer: Strip transformer for fast image deblurring. In *ECCV*, 2022. 2
 [20] Ashish Vaswani, Noam Shazeer, Niki Parmar, Jakob Uszkoreit, Llion Jones, Aidan N. Gomez, Lukasz Kaiser, and Illia Polosukhin. Attention is all you need. In *NIPS*, 2017. 2

- [21] Zhendong Wang, Xiaodong Cun, Jianmin Bao, Wengang Zhou, Jianzhuang Liu, and Houqiang Li. Uformer: A general u-shaped transformer for image restoration. In *CVPR*, 2022. [2](#)
- [22] Tao Yang, Rongyuan Wu, Peiran Ren, Xuansong Xie, and Lei Zhang. Pixel-aware stable diffusion for realistic image super-resolution and personalized stylization. *arXiv preprint arXiv:2308.14469*, 2023. [2](#), [3](#), [5](#)
- [23] Fanghua Yu, Jinjin Gu, Zheyuan Li, Jinfan Hu, Xiangtao Kong, Xintao Wang, Jingwen He, Yu Qiao, and Chao Dong. Scaling up to excellence: Practicing model scaling for photo-realistic image restoration in the wild. In *CVPR*, 2024. [2](#), [3](#)
- [24] Lu Yuan, Jian Sun, Long Quan, and Heung-Yeung Shum. Image deblurring with blurred/noisy image pairs. *ACM Trans. Graph.*, 26, 2007. [2](#)
- [25] Syed Waqas Zamir, Aditya Arora, Salman Khan, Munawar Hayat, Fahad Shahbaz Khan, Ming-Hsuan Yang, and Ling Shao. Multi-stage progressive image restoration. In *CVPR*, 2021. [2](#)
- [26] Syed Waqas Zamir, Aditya Arora, Salman Khan, Munawar Hayat, Fahad Shahbaz Khan, and Ming-Hsuan Yang. Restormer: Efficient transformer for high-resolution image restoration. In *CVPR*, 2022. [2](#), [3](#), [6](#), [7](#)
- [27] Hongguang Zhang, Yuchao Dai, Hongdong Li, and Piotr Koniusz. Deep stacked hierarchical multi-patch network for image deblurring. In *CVPR*, 2019. [2](#)
- [28] Lvmin Zhang, Anyi Rao, and Maneesh Agrawala. Adding conditional control to text-to-image diffusion models. In *ICCV*, 2023. [3](#)
- [29] Shaojie Zhuo, Dong Guo, and Terence Sim. Robust flash deblurring. In *CVPR*, 2010. [2](#)